EB11

19th International Symposium of Ballistics, 7–11 May 2001, Interlaken, Switzerland

AERODYNAMIC ASPECTS OF A GRID FINNED PROJECTILE AT SUBSONIC AND SUPERSONIC VELOCITIES

A. Dupuis[1] and C. Berner[2]

[1]Precision Weapons Section, Defense Research Establishment Valcartier (DREV), Val-Belair, Quebec, Canada, G3J 1X5
[2]Aerodynamics and Acoustics Division, French-German Research Institute (ISL), Saint-Louis, France

Wind tunnel tests were conducted on a grid finned projectile configuration in the Mach number range of 0.6 to 3.0. The four fins consisted of nine cells in a vertical orientation. They were located 0.7 cal ahead of the base of an ogive-cylinder body with a length to diameter ratio of 10.0. Flow visualizations as well as force and moment measurements were conducted. The axial and normal forces, the static and roll moments were obtained for angles of fin cant of 0.0°, 5.0°, 10.0° and 15.0°. Free-flight drag data is also presented.

INTRODUCTION

The use of grid fins as a stabilization and control device on projectiles and missiles offers an interesting alternative to the classical fin design. Their easy storage for deployment, low hinge moments and high angle of attack performance are their main advantages while their main shortcoming is a higher drag penalty.

A joint project was undertaken between France and Canada to increase the knowledge base of projectiles and missiles equipped with grid fins. The objectives of this work were to study the fundamental aerodynamics phenomena associated to this type of control surfaces and to compare these results with other types of conventional control such as lateral and/or impulse jets and classical planar lifting surfaces. Furthermore, the database generated during this investigation will be used to point out the advantages and disadvantages of such a concept compared to other ones. They also will constitute test cases to validate numerical prediction codes.

Results contained in this paper were produced from two test series conducted on models at the ISL supersonic wind tunnel and the DREV trisonic wind tunnel and some drag data obtained from free-flight tests conducted at DREV.

MODEL CONFIGURATION

The reference configuration was the Air Force Finner [1] body equipped with four grid fins, as shown in Fig. 1a. The body consisted of a 2.5 caliber tangent-ogive followed by a 7.5 caliber cylinder. The fins were placed at 0.7 calibers from the base. The total span is 2.4 calibers with a chord of 0.08 calibers.

The grid fin, presented in Fig. 1b, has nine cells with thick walls. Thick walls were chosen to allow wind tunnel static wall pressure measurements on the central cell. This grid fin geometry, contrary to many other papers [2–4], has a vertical cell orientation instead of a cruciform one. This was done to simplify the geometry to be able to understand basic aerodynamic phenomena of simple cells. Each cell is rectangular with a width of 0.124 caliber and a height of 0.161 caliber. In order to avoid possible structure deficiencies during free-flight tests, a solid base was designed to mount the fins on the body. The first model, defined as the reference configuration, had zero fin deflection angle on all four devices. Three other configurations had all four fins canted at 5, 10 and 15 degrees, respectively, to produce a pure roll motion.

EXPERIMENTAL PROCEDURE

Experimental facilities

The wind tunnel experiments were conducted in the DREV trisonic 60 cm x 60 cm wind tunnel [5] and the French-German Research Institute of Saint-Louis (ISL) blow down facility with a test section of 20 cm x 20 cm. The facilities are further described in [7].

Test Procedures and Techniques

The wind tunnel models tested at DREV and ISL were supplied by ISL and they had a diameter of 20 mm. The 12.7-mm Able balance was utilized for these experiments. The aerodynamic coefficients were obtained by best fit polynomials through the measured experimental data.

The DREV wind tunnel aerodynamic results (CA0, CN, Cm, Cl, Xcp) were obtained from a combination of model sweeps between –5° and +15° incidence at roll orientations of 0° and +45°. The tests were conducted at supersonic Mach numbers of 1.5, 2.0, 2.5 and 3.0 and at a nominal subsonic Mach number of 0.6. The slopes of the normal force and the pitching moment coefficients were obtained from the best-fit line through the experimental data between –5° and +5°. The axial force at zero angle of attack, CA0, is uncorrected for base effects, i.e. it is the value as measured by the balance. The roll moment due to fin cant (Clδ) provided, is the one measured at zero angle of attack.

ISL results include shadowgraph flow visualizations, force and moment measurements at a nominal Mach number of 3.0. Flow visualizations were conducted for 3 fin configurations (one shown in this paper, $\delta = 0.0$) at angles of attack ranging between zero and 12° at zero and 45° roll orientation. Forces and moments were obtained using the same test procedures as for the DREV wind tunnel.

FREE-FLIGHT TESTS

Two series of free-flight tests were conducted to assess the launch of the models from a 110-mm smooth bore gun before testing in the DREV aeroballistic range. The main goal of these tests is to verify the sabot-model integrity at launch and to make sure that the model is stable over a distance of 250 m, the length of the aeroballistic range. Doppler radars were used on these trials to obtain the velocity of the projectiles as they flew down range. The drag data was then extracted. The model diameter was 30.0 mm and one set of fins were canted at 2.0° to produce roll and the other set was deflected at 0.5° to create a trim.

The models for the first series of free-flight tests had a brass nose and for the second series, the nose was made of tungsten to shift the center of gravity forward due to stability aspects, as explained below. The total drag was calculated from the retard of the projectiles over a distance of roughly 250 m.

FLOW VISUALIZATION

Fig. 2 shows some typical shadowgraph examples for the projectile with no fin cant for a Mach number of 3.0 at 0 and 12 degrees angle of attack and at zero roll orientation. The figures show how the flow field is highly complicated due to the interaction between grid cells as well as the interaction between the grid fins and the body. Fig. 3 represents a schematic of the flow structure near a single fin at α=0°. At zero angle of attack, after the attached nose shock, clearly seen in Fig. 2a, the boundary layer increases and flow along the body separates. This separation generates a recompression shock (1) in front of the grid fin triggered by the recirculating region (2) generated by, in our case, the solid fin attachment. Due to this region, the flow is deviated and it collapses with the grid fin under an incidence close to the angle of shock (1). At high Mach numbers, flow through the cells is started (swallowed) and the normal bow shock (3') observed in front of the fins is generated by the different webs and not by a unique choked flow located in front of the grid fin. Shock (3") is the upper part of the bow shock generated by the top web.

Behind the fin, one can see a first shock (4) generated by the base of the top web followed by multiple shock waves (5) and expansions whose origin are due to the front recompression and web bow shocks passing through each single grid cell or by the shocks generated by the small near-wakes (6) behind each web. Close to the body, a near-wake recompression shock (7) is triggered by the base recirculating region (8) behind the fin attachment. Shock generated by the fins located at a 90° roll angle (not represented in Fig. 3) can also be observed.

Fig. 2b shows the same configuration at an angle of attack of 12°. The attached shock is, as expected, more intense on the windward side and the shock system in front and behind the grid fins is asymmetric and even more complicated than for zero angle of attack. Along the body, the flow is also separated and interacts with the upper fin and therefore decreases the efficiency of that fin. Aerodynamics of grid fins are so complex that it is very difficult to draw definite conclusions from the flow visualization. The planned CFD predictions and experimental wind tunnel tests to be carried out on an up-scaled (x4) single grid fin mounted in the test section on a partially cylindrical splitter plate might help to better understand the flow features around this type of fin configurations.

AERODYNAMIC COEFFICIENTS

Due to lack of space, only the aerodynamic coefficients then CA0, CNα, Cmα, Clδ, and XCP0 will be presented as a function of Mach number over the whole Mach number range tested. Angle of attack variations as well as other fin deflections can be found in [7].

Zero Yaw Axial Force Coefficient

The axial force coefficient vs. Mach Number is shown in Fig. 4. CA is of the order of 0.9 to 1.2, and these magnitudes were expected [2, 3]. This is one of the principal concerns of using grid fins. However, altering the cross section shape on the outer frame and the web design [2] can reduce this high drag coefficient. In general, the trend of CA0 is that of conventional planar fins [1]. The results also show an increase of CA0 of 20% when the fins are deflected at 15° as compared to no deflections. This increase is observed over the whole Mach number range.

There is a difference in the measured CA0 between DREV and ISL at Mach 3.0. The ISL result is roughly 15.0 % higher than the DREV measured value. The boundary layer in the DREV wind tunnel is laminar while it is turbulent in the ISL one. Previous wind tunnel tests at Mach 2.5 on a clipped delta fin projectile [6] did not show large differences as this one. Therefore, it is believed that the difference shown here is due to the particular grid fin and its sensitivity to the boundary layer type.

The total drag coefficients obtained from the two series of free-flight tests are also shown in the figure. The order of magnitude and the trend agree quite well with the wind tunnel data. At roughly Mach 2.5, there is a slight difference in the free-flight drag data, but this is probably due angle of attack effects.

Normal force coefficient

Fig. 5 presents the normal force coefficient slope, CNα as a function of Mach number. In this case, there was only a difference of about 11% between the DREV and ISL measured values at Mach 3.0. The first trend to observe is that CNα increases as the Mach number increases. This implies that the fins become more effective as the Mach number increases while standard planar fins [1] usually have the opposite trend. At Mach 1.5, all four configurations have the same CNα value. Supersonically, the fin effectiveness decreases as the fin deflection increases and this difference increases with Mach number. Subsonically, the trend is the opposite of the supersonic one. That is, the fins are more effective at 0° deflection than at 15°. Also, subsonically, there is almost a factor of 2.0 in CNα between fins not deflected and those deflected at 15°.

Static pitch moment coefficient

Fig. 6 presents the Mach number effects on the pitching moment coefficient slope Cmα. The reference location for Cmα is about the center of gravity, which is located 4.03 calibers from the nose of the projectile. In this case, there was a 20.0% difference in the measured values between DREV and ISL at Mach 3.0. As for CNα at Mach 1.5, Cmα is the same four all four fin deflections. Supersonically, the static stability increases with increasing Mach number. This trend is also opposite of the behavior of a planar fin. Supersonically, the static stability decreases as the fin deflection increases and this difference increases with Mach number. At Mach 3.0, there is a factor of 2.0 in Cmα when the fins are deflected at 15° and when they are not. An unexpected result was seen at Mach 0.6. The projectile is statically unstable when the fins are deflected at 0° and 5°, marginally stable at 10° and statically stable when all four fins are deflected at 15°. As for CNα, the trend is again opposite of the supersonic one.

Center of Pressure

The center of pressures (about the base of the projectile) from the experimental tests are compared vs. Mach number in Fig. 7. Supersonically, XCP0 is again the same at Mach 1.5 for all four fin deflections, and just aft of the center of gravity. XCP0 moves to the back of the projectile towards the fins, which implies that the projectile becomes more stable, with increasing Mach number. The static stability, defined as the difference between the center of pressure and the center of gravity, is decreasing with increasing fin deflection and this difference increases with Mach number. For example at Mach 3.0, there is a one-caliber difference in XCP0 when the fins are fully deflected and when they are not. For the same Mach number, the ISL XCP0 is located at 0.4 caliber more towards the nose of the projectile than the DREV measured value.

The most interesting results in this case occur subsonically. When the fins are not deflected, the center of pressure is located in front of the projectile. As the fin deflection increases, XCP0 moves backward along the projectile, and it is behind the center of gravity only when all four fins are fully deflected at 15°. There is almost a five caliber displacement of the center of pressure with fin deflection. This means, with no doubt, that subsonically, the static stability of this grid fin configuration is very sensitive to the fin deflection.

Roll Moment Coefficient

Fig. 8 shows the evolution of the roll moment coefficient Clδ due to the fin deflection vs. Mach number. The configuration with no deflections, of course, produced no roll moment or very small values. The values supplied were taken at zero angle of attack.

Supersonically, Clδ increases linearly with Mach number and this was expected since the normal coefficient slope CNα increases also with Mach number. Again this trend is opposite of planar fins. In addition, Clδ is not linear with the fin deflection angle. More so, the roll producing moment is less effective as the fin deflection increases.

Once more, subsonically, an interesting result is observed. When the fins are deflected at 10° and 15°, Clδ is negative and it is positive when the fins are deflected at 5°, indicating a roll reversal. This result, not shown here, was also seen when the model was oriented at a roll angle of 45°.

CONCLUSION

A detailed wind tunnel experimental investigation was conducted for a grid finned projectile configuration with fins deflected at different angles and for Mach numbers ranging from 0.6 to 3.0. Incidence varied for angles between -15° and +15° and fin roll orientations were of 0o and 45o. Mach number dependencies on axial force, normal force, pitching moment, center of pressure location and roll moment were obtained. Drag data obtained from free-flight tests were also compared.

Overall, the trend of CNα and Cmα for the grid finned projectile is opposite of a standard planar finned projectile. That is, for a constant fin deflection, the effectiveness of the fins and the static stability increases as the Mach number increases, supersonically. On the other hand, subsonically (at Mach 0.6), the projectile is statically unstable while for a planar fin, it is statically stable.

The results showed that all the aerodynamic coefficients were very sensitive to the deflection angle of the fins, and at the same Mach number, there were large differences in the results. As well, the trend with Mach number was reversed when going from subsonic to supersonic.

One very interesting result was observed subsonically. When the fins were not deflected, the center of pressure was located in front of the projectile, and when the fins were deflected, it shifted towards the back of the model.

A roll reversal was detected at Mach 0.6 that was dependent on the fin deflection.

These results are not only a very important set of aerodynamic force and moment coefficients that describes the behavior of grid fin technology. They constitute a reliable database that can be used as a reference for the validation of CFD codes or empirical/analytical tools. The use CFD coupled to wind tunnel tests on a single grid fin mounted on a splitter plate will certainly be a most promising tool for the analysis of flow conditions around the grid fins and inside the grid cells. Aeroballistic range free flight tests will be carried out in the near future and the present experimental data and CFD analysis will be compared with those results.

REFERENCES

1. West, K. O., “Comparison of Free-flight Spark Range and Wind Tunnel Test Data for a Generic Missile Configuration at Mach Numbers From 0.6 to 2.5”, AFATL-TR-81-87
2. Washington, W.D., Miller, M.S., “Experimental Investigations on Grid Fin Aerodynamics: A Synopsis of Nine Wind Tunnel and Three Flight Tests”, RTO-MP-5 AC/323(AVT)TP/3, November 1998
3. Simpson, G.M., Saddler, A.J., “Lattice Controls: A Comparison with Conventional Planar Fins”, RTO-MP-5 AC/323(AVT)TP/3, November 1998

4. Abate, G.L., Duckerschein, R.P., Hathaway, W., "Subsonic/Transonic Free-Flight Tests of a generic Missile with Grid Fins", AIAA Paper 2000-0937, 38th AIAA Aerospace Sciences Meeting and Exhibit, Reno, NV, USA, Jan. 2000
5. "Commissioning Report of the DREV 2 ft Indraft Tunnel", Dilworth, Secord, Meagher and Associates Ltd, Report No. 695/912, March 1977.
6. Berner C., Dupuis, A. "Wind Tunnel Investigation and Analysis of the DREV-ISL Reference Projectiles", DREV-R-9520, June 1996
7. Berner, C., Dupuis, A., "Wind Tunnel Tests of a Grid Finned Projectile Configuration", AIAA 2001-0105, 39th Aerospace Sciences Meeting Reno, Nevada, 8–11 Jan 2001

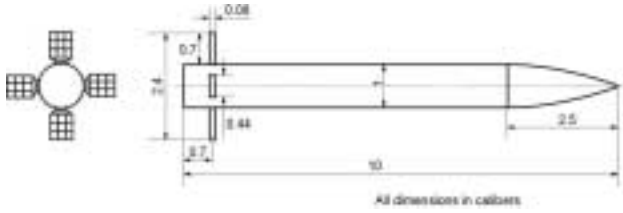

Fig. 1a: Body.

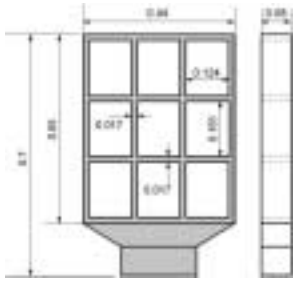

Fig. 1b: Grid fin details.

Figure 1: Grid fin projectile configuration (caliber, 1 cal = 20 mm).

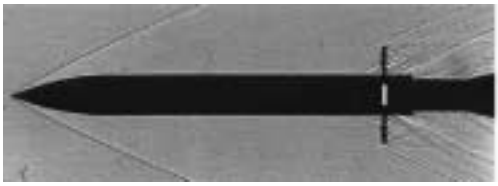

Fig. 2a: Angle of attack = 0.0°.

Fig. 2b: Angle of attack = 12.0°.

Figure 2: Shadowgraph of projectile with δ = 0.0° (M = 3.0).

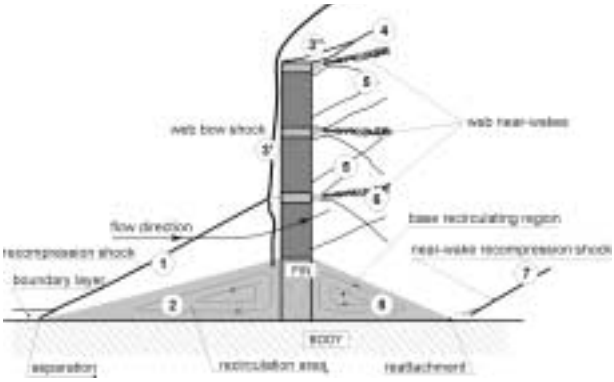

Figure 3: Schematic of flow structure.

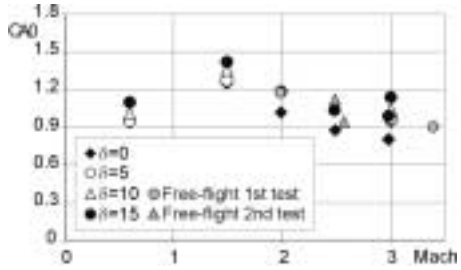

Figure 4: Axial force coefficient.

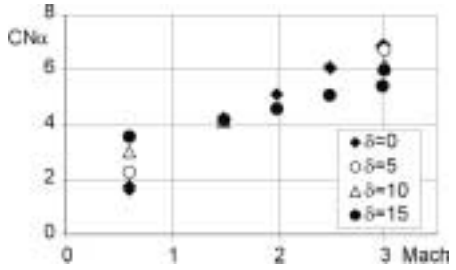

Figure 5: Normal force coefficient slope.

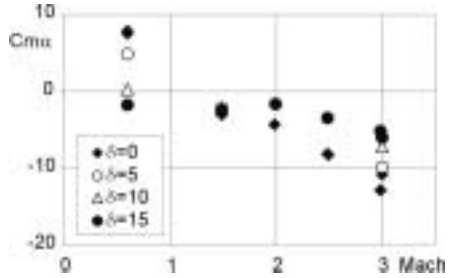

Figure 6: Pitch moment coefficient slope.

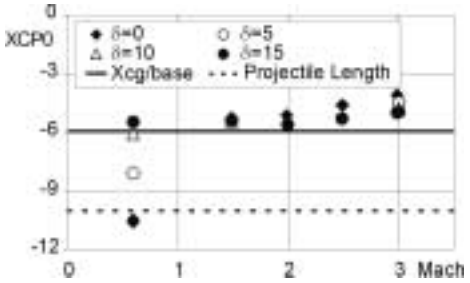

Figure 7: Center of pressure (cal from base).

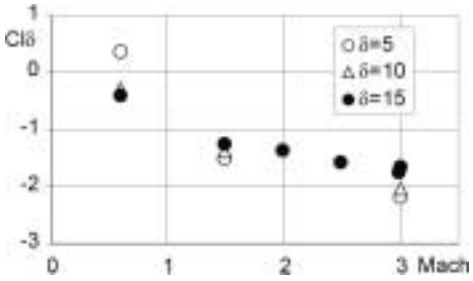

Figure 8: Roll moment due to fin cant.